

## 太赫兹多波段的电磁诱导透明设计与分析

张敏, 延凤平\*, 杜雪梅, 仇晓琦

北京交通大学光波技术研究所全光网络与现代通信网教育部重点实验室, 北京 100044

**摘要** 设计了一种超材料三维模型,由闭合方环和 4 个开口谐振方环通过正、反向双开口方环与闭合方环相互耦合来组成,在太赫兹范围内具有多波段电磁诱导透明(EIT)效应。该结构分别实现了在 1.21、1.46、1.61、1.98 THz 这四波段的电磁诱导透明现象,并且谐振强度均达到 0.9 左右。通过将结构单元进行拆分并相互对比分析,研究了该超材料结构产生多波段 EIT 效应的物理机理,并重点分析了开口大小、闭合方环尺寸对 EIT 强度与带宽的影响。通过对三维立体结构仿真分析可知,所设计的超材料不仅在多个波段获得了较高的折射率灵敏度,还具有高强度、多频点的慢光效应。因此,其在折射率传感与光缓存器件等领域,具有良好的应用前景。

**关键词** 材料;超材料;电磁诱导透明;多波段;太赫兹;慢光效应

中图分类号 O436

文献标志码 A

doi: 10.3788/CJL202148.0314001

## 1 引言

相对于自然材料,通过人工合成周期性单元结构所诞生的超材料<sup>[1]</sup>,优势在于能够通过设计来实现诸如电磁诱导透明(EIT)、近零折射率、光子禁带等特殊的电磁现象<sup>[2-4]</sup>。因此,通过合理的材料选型与结构参数调整来实现超材料性能上的提升已成为行业内的关注热点,从而促进了超材料器件在太赫兹技术<sup>[5-6]</sup>领域的广泛应用。

EIT<sup>[7-10]</sup>是一种光量子干涉相消效应,使不透明介质对探测光具有透明效果<sup>[11-12]</sup>,该特性在实现慢光方面具有重要应用价值<sup>[13-14]</sup>。在原子领域,传统实现 EIT 效应时,通常要求超低温、强光抽运等严苛的实验条件<sup>[15]</sup>,而利用超材料实现 EIT 效应时,只需要明、暗模式结构,二者谐振吸收频率相近,电磁波入射后,相互耦合,透射峰随之出现。此后,以不同结构的超材料为对象,以实现电磁诱导透明现象为目标的研究成果被陆续提出。2009 年, Liu 等<sup>[16]</sup>提出了一种基于不同介质的双层超材料结构在亮暗模耦合下,实现 EIT 现象。2010 年, Kim 等<sup>[17]</sup>设计的超材料结构,由双金属圆环构成,在太赫兹波段产生峰值较尖锐的 EIT 透射峰。与单频

相比,多频段宽带 EIT 通常较难实现。2014 年, Ding 等<sup>[18]</sup>研究了具有单个和多个透明窗口,并且可以通过改变石墨烯层的费米能级来动态控制多个透明度窗口的可调石墨烯等离激元超材料。2015 年, Hu 等<sup>[19]</sup>研究了具有有限金属条和一个双开口谐振环(SRR)的平面超材料的传输特性,结果表明,两个金属带之间的长度差可导致微波区域的双频带 EIT 光谱响应,如果两个金属带的长度相等,则金属带对仅显示单个共振。2018 年, Ning 等<sup>[20]</sup>在由石墨烯带(GR)和 LiF 平板组成的石墨烯超表面的复合结构中实现了多频带和宽带 EIT 效应,以上对超材料 EIT 效应的研究大多采用平面结构。

本文设计了一种由闭合方环(SCL)和 SRR 构成的三维超材料模型结构。通过借助 CST Microwave Studio 电磁仿真分析平台,分别对模型结构所包含的正向双开口方环(FSRR)、反向双开口方环(RSRR)与闭合方环进行互相电磁耦合与单独电磁耦合的数值仿真分析,探究其在太赫兹波段实现 EIT 效应的物理机理,并对该结构在慢光效应与折射率传感方面的应用进行了研究。与当前领域内研究相比,该超材料三维立体模型实现了多波段的高折射率灵敏度,多个频点的慢光效应,在折射率

收稿日期: 2020-07-16; 修回日期: 2020-09-05; 录用日期: 2020-09-14

基金项目: 国家自然科学基金(61327006,61620106014)

\*E-mail: fpyan@bjtu.edu.cn

传感<sup>[21-23]</sup>与光缓存器件<sup>[24]</sup>等领域,具有良好的应用前景。

## 2 单元结构设计

图 1 为基本单元结构,多波段 EIT 超材料的石英基底厚度  $d=20\ \mu\text{m}$ ,介电常数  $\epsilon=3.75$ ,单元周期  $p=150\ \mu\text{m}$ 。垂直布置于石英基底上有 4 个谐振方环,其参数相同,开口互为正、反向。材质选用金

属铜,电导率  $\sigma=5.8\times 10^7\ \text{S/m}$ ,外边长  $L_1=30\ \mu\text{m}$ ,内边长  $L_2=20\ \mu\text{m}$ ,金属线宽  $w=5\ \mu\text{m}$ ,开口大小  $g=4\ \mu\text{m}$ ,方环间距  $s=40\ \mu\text{m}$ 。厚度  $t=5\ \mu\text{m}$  的闭合方环位于基底水平面上,外径边长  $a=74\ \mu\text{m}$ ,内径边长  $b=64\ \mu\text{m}$ ,可与开口方环实现立体耦合的作用。对图 1(a) 超材料三维结构分别施加垂直方向的电场  $E$  和水平方向上的磁场  $H$ ,入射电磁波方向  $S$  与闭合方环表面垂直。

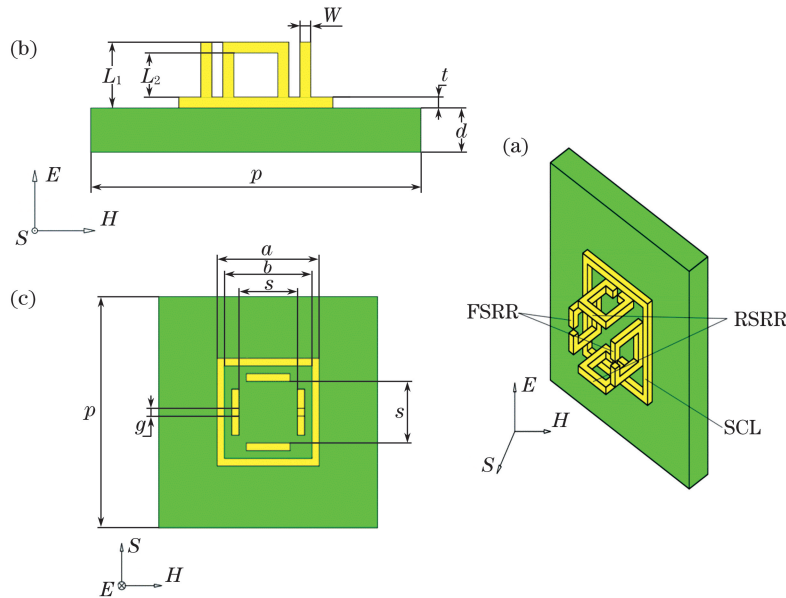


图 1 结构图。(a)超材料三维图;(b)侧视图;(c)正视图

Fig. 1 Structural drawing. (a) Three-dimensional view of metamaterials; (b) side view; (c) front view

## 3 多波段 EIT 超材料机理分析

为分析所设计的 EIT 超材料结构对入射电磁波的响应情况及该结构多波段 EIT 效应的产生机理。对图 1 所示的完整结构,去掉反向双开口环得到结构 I,去除正向双开口环得到结构 II,利用 CST 分别进行仿真分析,得到的 S 参数频谱图如图 2 所示。

图 2 分别表示完整结构、结构 I、结构 II 对入射电磁波的响应情况。其中,实线的仿真对象是超材料的完整结构,仿真结果出现 4 个透射峰频点,分别在 1.21、1.46、1.61、1.98 THz 处,结构体中作为明模与暗模的耦合体分别是正、反向双开口与闭合方环,且其谐振强度分别为 0.90、0.89、0.90、0.87;短点线是结构 I 的仿真结果,透射峰分别出现在 1.43 THz 与 1.64 THz 频点处,它的明模与暗模的耦合结构分别是正向双开口环与闭合方环。短划点是结构 II 的耦合仿真结果,谐振峰出现在 1.32 THz 和 1.59 THz 频点处,结构中的反向双开

口环与平面闭合方环分别作为明模与暗模。以上仿真结构相比于传统结构,实现了四波段、高强度的 EIT 效应。

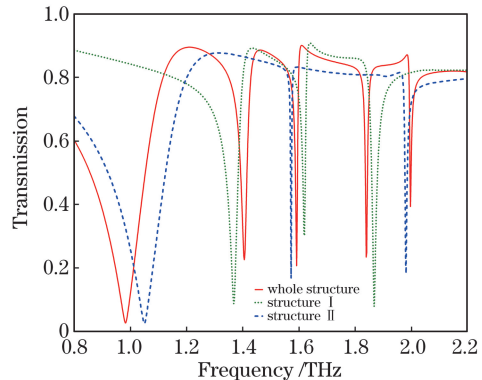


图 2 三种结构的 EIT 频谱图

Fig. 2 EIT spectrogram of three structures

为了进一步分析上述谐振峰的产生机理,绘制图 1 完整结构分别在 1.21、1.46、1.61、1.98 THz 这四个频点处的电磁场分布,如图 3 所示。

第一个谐振透射峰出现在 1.21 THz 处,对比电

场分布图 3(a)与磁场分布图 3(e)所显示出的能量聚集情况,可以推断出正、反向双开口环与闭合方环互为明、暗模,在磁波入射后发生耦合而得。第二个透射峰出现在 1.46 THz 处,对比电场分布图 3(b)和磁场分布图 3(f)中的能量聚集情况,在电磁波入射后,由正向双开口环与闭合方环互为明、暗模耦合所得。第三个透射峰位于 1.61 THz 处,对比电场分布图 3(c)和磁场分布图 3(g)显示的能量聚集情况,它是由 4 个开口环与闭合方环互为明、暗模耦合所得。最后一个透射峰出现在 1.98 THz 处,对比电场分布图 3(d)和磁场分布图 3(h)中的能量聚集情况可以得出,它是由反向双开口环与闭合方环互为明、暗模耦合所得。

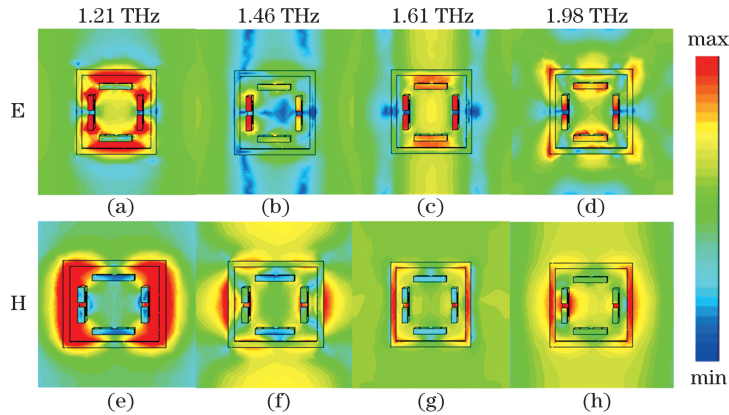


图 3 EIT 各谐振峰值处电磁场分布图。(a)~(d)电场分布;(e)~(h)磁场分布

Fig. 3 Electromagnetic field distribution diagrams at each resonance peak of EIT. (a)~(d) Electric field distribution diagrams; (e)~(h) magnetic field distribution diagrams

## 4 结构参数与特性分析

### 4.1 宽带 EIT 特性

分别单独对正、反向双开口环与闭合方环进行谐振响应分析,并将出现在 1.21 THz 和 1.61 THz

处的宽带透射峰的仿真结果与图 2 中的结构 I、II 的仿真结果作对比,得出如图 4 所示的仿真结果。

除闭合方环的电磁波谐振响应是在单一频点 1.19 THz 处之外,正向双开口环有 1.48 THz 和 1.96 THz 两处的电磁波谐振频率;反向双开口环有

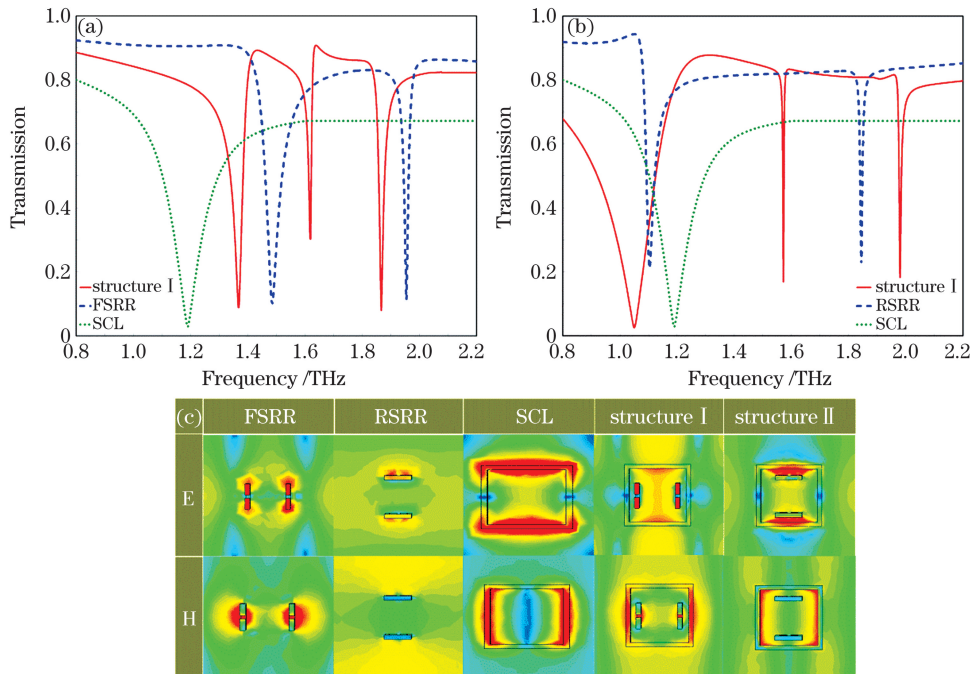


图 4 正、反向开口环与结构 I、II 的对比图。(a)正向双开口环;(b)反向双开口环;(c)单独结构的电磁场分布

Fig. 4 Comparison of positive and negative split rings with structures I and II. (a) Forward double split ring; (b) reverse double split ring; (c) electromagnetic field distribution of separate structure

1.10 THz 和 1.84 THz 两处的电磁波谐振频率。结合以上单独结构下的电磁场分布[图 4(c)],皆能在上述谐振频率点处出现强烈的电磁谐振现象,进而得出吸收峰如图 4(a)、(b)所示。通过比较吸收峰,正向双开口环较闭合方环更尖锐,故电磁谐振更强烈,  $Q$  值(谐振的中心频率与  $-3$  dB 带宽的比值)也更高,具体见图 4(a)中横向与纵向的短点线。因此,正向双开口环与闭合方环互为明、暗模式并耦合形成带宽均能达到 0.25 THz(所述“带宽”定义为透射峰两波谷的间距)的两个透射峰。而图 4(b)中,反向双开口环与闭合方环互为明、暗模式,耦合形成带宽分别为 0.52 THz 和 0.41 THz 的两个透射峰。对比传统窄带结构的 0.1 THz 带宽,上述仿真结果的宽带特性优势较明显。

由于入射电磁波与正向双开口环发生谐振会引起剧烈的能量变化,这与电磁场分布图 4(c)中的 FSRR、RSRR 仿真结果相符,故闭合方环与正向双开口环耦合所得的 EIT 谐振强度也会更高。

#### 4.2 开口大小

为研究 EIT 受超材料结构参数影响情况,如图 5 所示,通过调节开口方环的开口参数大小  $g$ ,得出  $g$  是第二、第三个 EIT 透射峰的关键参数。如实线所示,在  $g=4.0 \mu\text{m}$  时,第二透射峰谐振强度为 0.89,带宽为 0.17 THz,第三透射峰谐振强度为 0.90,带宽为 0.26 THz;并且 EIT 透射峰谐振强度随着参数  $g$  递增而呈现逐渐降低的趋势,带宽也随之减小;当  $g=6.4 \mu\text{m}$  时,如短划线所示,超材料结构产生的 EIT 透射峰谐振强度下降到 0.85 以下。

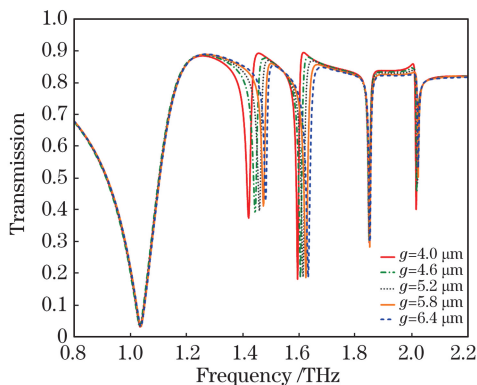


图 5 开口大小对 EIT 效应的影响

Fig. 5 Effect of opening size on EIT effect

#### 4.3 闭合方环尺寸

进一步,观察图 4(c)中平面闭合方环结构

(SCL)的电磁场分布可知,闭合方环与入射电磁波发生单独谐振响应时,能量变化剧烈,可见 EIT 效应还与闭合方环尺寸有关。如图 6 所示,通过等比例调节闭合方环尺寸所得出的 EIT 透射峰变化的仿真结果显示,参数  $a$  的变化对由 4 个开口方环与闭合方环耦合产生的第一个透射峰影响显著。其中,在  $a=66 \mu\text{m}$  时,透射峰谐振强度随着  $a$  的递增而逐渐增大,表现为透射峰小幅蓝移,带宽也随之增大。如图中实线所示,在  $a=74 \mu\text{m}$  时,透射峰谐振强度可达 0.9,带宽为 0.43 THz。

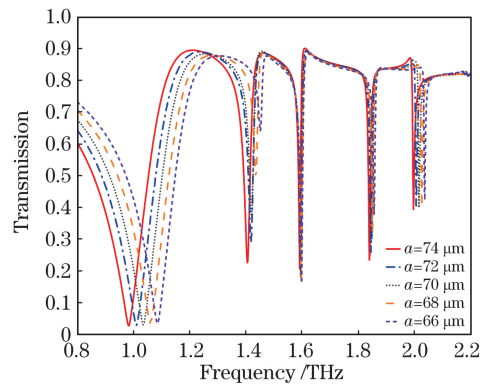


图 6 闭合方环尺寸对 EIT 效应的影响

Fig. 6 Influence of closed square ring size on EIT effect

## 5 光缓存与传感应用分析

### 5.1 光缓存

谐振峰强度对超材料结构在光缓存器件中的应用有重要影响,由于金属损耗的存在,如何提高谐振强度,进而提高群折射率成为了问题的关键。为此,对所设计结构产生的群折射率变化进行了仿真分析。所研究的超材料的慢光效应是伴随 EIT 效应产生过程中入射电磁波的折射率骤增、色散强烈进而导致其波速减小,甚至为 0。因此,适合应用于光缓存器件领域。

电磁波的群折射率的表达式为

$$n_g = \frac{c}{\nu_g} = n + \omega \frac{dn}{d\omega}, \quad (1)$$

式中:  $dn/d\omega$  表明介质色散大小与折射率随角频率的变化有关,其余参数  $c$ 、 $\nu_g$ 、 $\omega$  分别为真空光速、波包群速度和角频率。而通过 S 参数反演算法<sup>[25-29]</sup>得出介质折射率的表达式为

$$n = \frac{1}{kd} \cos \left[ \frac{1}{2S_{21}} (1 - S_{11}^2 + S_{21}^2) \right], \quad (2)$$

式中:  $k$  为单位周期内电磁波的个数(即  $k=2\pi/\lambda$ );  $d$  为介质的厚度;  $S_{11}$ 、 $S_{21}$  为介质中电磁波的反射率

与透射率,可由 CST 电磁仿真软件算出; $n_g$  为慢光效应强度,其值越大表明电磁波群速度(复合光速度) $v_g$  越小。CST 软件仿真结果如图 2 所示,其中完整结构的折射率曲线可根据(2)式得出,图 7(b)中的群折射率曲线是通过(1)式计算得出的。

结合图 7 的仿真结果可知,四波段 EIT 效应分别产生于 0.98, 1.41, 1.60, 1.84, 1.99 THz 这 5 个

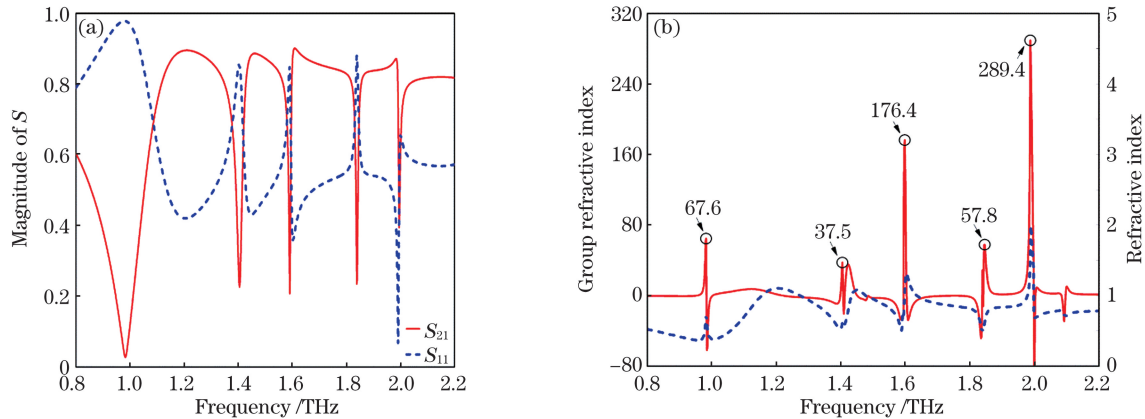


图 7 多频点慢光效应频谱图。(a) S 参数;(b)群折射率、折射率随频率的变化

Fig. 7 Spectrogram of slow light effect at multiple frequencies. (a) S parameter; (b) group refractive index and refractive index change with frequency

## 5.2 折射率传感器

EIT 超材料结构中,明模式与暗模式相互耦合,会根据周围环境折射率的变化产生不同的谐振峰频率,因而能够应用于折射率传感器的制作选材。仿真过程中设置折射率从 1~3 变化并设定所涂覆分析物厚度为  $3 \mu\text{m}$ ,对图 1 结构进行因折射率变化而导致谐振峰频率变化的仿真,结果

透射谷频点之间。在 EIT 效应中,伴随着折射率与色散的迅速增大,群折射率也随之增大,其值分别为 67.6、37.5、176.4、57.8、289.4。尤其是在群折射率较高的 176.4 和 289.4 频点处,慢光效应更加强烈。与之前超材料结构<sup>[30]</sup>作对比,所设计的超材料结构能够覆盖更高的频段,具有更多的慢光效应频点,其应用价值不言而喻。

如图 8(a) 所示。图中透射峰的红移现象是周围介质折射率增大而引起的。计算得到 4 个频段的折射率灵敏度分别为 235.2、392、658、294 GHz/RIU,其值对比文献<sup>[31]</sup>(60.69 GHz/RIU)有明显的提升。因此,本文研究设计的超材料结构对比传统的 EIT 结构,不仅具有多波段的折射率传感性能,而且灵敏度也较高。

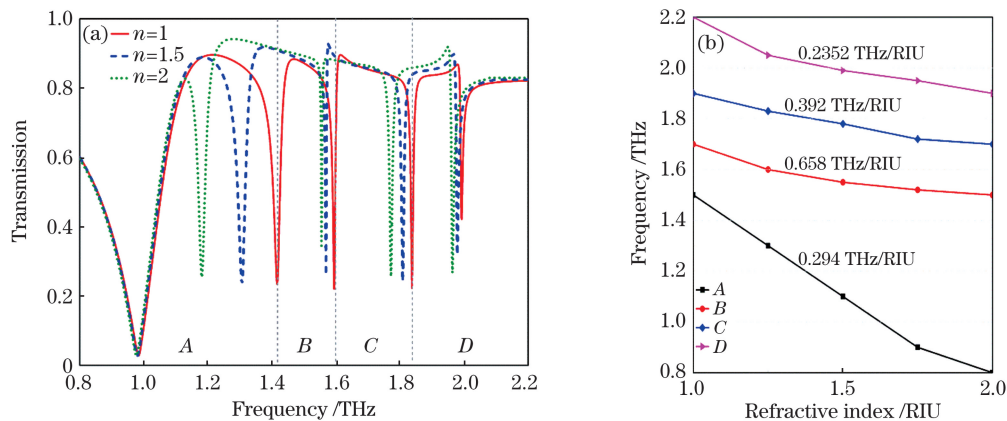


图 8 多波段折射率传感频谱图。(a)不同折射率下的 EIT 曲线;(b)4 个波段的折射率灵敏度

Fig. 8 Multi-band refractive index sensing spectrogram. (a) EIT curves at different refractive indices; (b) refractive index sensitivity in four bands

## 6 结 论

本文研究结果表明在太赫兹波段内,所设计的

超材料三维结构模型可实现 1.21、1.46、1.61、1.98 THz 四频点的 EIT 效应,且谐振强度分别达到 0.90、0.89、0.90、0.87。通过对比正、反向双开

口方环与闭合方环的耦合响应,研究了多波段 EIT 谐振产生的机理。通过调节结构参数,讨论了超材料中开口谐振方环的开口大小、闭合方环尺寸对 EIT 强度与带宽的影响。相比于传统的设计,本文设计的超材料三维结构具有多波段 EIT 效应,并在多个波段下具有较高的折射率灵敏度,能够在多个频点处产生强烈的慢光效应。因此,其适宜在折射率传感与光缓存领域应用与推广。

### 参 考 文 献

- [1] Zhang C H, Wu J B, Jin B B. Research progress on terahertz superconducting artificial electromagnetic metamaterials[J]. Chinese Journal of Lasers, 2019, 46(6): 0614005.  
张彩虹, 吴敬波, 金飏兵. 太赫兹超导人工电磁超材料的研究进展 [J]. 中国激光, 2019, 46(6): 0614005.
- [2] Li S X, Zhao H W, Han J G. Terahertz metamaterial sensor based on electromagnetically induced transparency effect[J]. Journal of Electronic Science and Technology, 2015, 13(2): 117-121.
- [3] Pan W, Yu X, Zhang J, et al. Absorption characteristics analysis of a terahertz metamaterial absorber based on double split square patches [J]. Applied Laser, 2016, 36(3): 346-350.  
潘武, 余璇, 张俊, 等. 基于双开口方形薄片的太赫兹超材料吸收器吸收特性分析 [J]. 应用激光, 2016, 36(3): 346-350.
- [4] Mao Q J, Feng C Z. Absorbance properties of nested-ring metamaterial absorbers based on magnetic polaritons[J]. Acta Optica Sinica, 2019, 39(8): 0816001.  
毛前军, 冯春早. 基于磁激元的嵌套环超材料吸波器的吸收特性 [J]. 光学学报, 2019, 39(8): 0816001.
- [5] Sun Y R, Chen H, Li X J, et al. Electromagnetically induced transparency in planar metamaterials based on guided mode resonance [J]. Optics Communications, 2017, 392:142-146.
- [6] Li D M, Yuan S, Yang R C, et al. Dynamical optical-controlled multi-state THz metamaterial absorber [J]. Acta Optica Sinica, 2020, 40(8): 0816001.  
李达民, 袁苏, 杨荣草, 等. 动态光调控多态太赫兹超材料吸收器 [J]. 光学学报, 2020, 40(8): 0816001.
- [7] Tassin P, Zhang L, Koschny T, et al. Planar designs for electromagnetically induced transparency in metamaterials [J]. Optics Express, 2009, 17(7): 5595-5605.
- [8] Dong Z G, Liu H, Cao J X, et al. Enhanced sensing performance by the plasmonic analog of electromagnetically induced transparency in active metamaterials[J]. Applied Physics Letters, 2010, 97(11): 114101.
- [9] Chen L, Gao C M, Xu J M, et al. Observation of electromagnetically induced transparency-like transmission in terahertz asymmetric waveguide-cavities systems [J]. Optics Letters, 2013, 38(9): 1379-1381.
- [10] Wang Y R, Liang L J, Yang M S, et al. Terahertz metamaterial based on controllable electromagnetic induced transparency structure [J]. Laser & Optoelectronics Progress, 2019, 56(4): 041603.  
王娅茹, 梁兰菊, 杨茂生, 等. 一种光控的电磁诱导透明太赫兹超材料 [J]. 激光与光电子学进展, 2019, 56(4): 041603.
- [11] Lukin M D, Imamoğlu A. Controlling photons using electromagnetically induced transparency[J]. Nature, 2001, 413(6853): 273-276.
- [12] Fleischhauer M, Marangos J P, Imamolu A, et al. Electromagnetically induced transparency: optics in coherent media [J]. Review of Modern Physics, 2005, 77(2): 633-673.
- [13] Vafapour Z, Alaei H. Subwavelength micro-antenna for achieving slow light at microwave wavelengths via electromagnetically induced transparency in 2D metamaterials[J]. Plasmonics, 2017, 12(5): 1343-1352.
- [14] Vafapour Z, Alaei H. Achieving a high Q-factor and tunable slow-light via classical electromagnetically induced transparency (CI-EIT) in metamaterials[J]. Plasmonics, 2017, 12(2): 479-488.
- [15] Zhu Z, Yang X, Gu J, et al. Broadband plasmon induced transparency in terahertz metamaterials [J]. Nanotechnology, 2013, 24(21): 214003.
- [16] Liu N, Langguth L, Weiss T, et al. Plasmonic analogue of electromagnetically induced transparency at the Drude damping limit [J]. Nature Materials, 2009, 8(9): 758-762.
- [17] Kim J, Soref R, Buchwald W R. Multi-peak electromagnetically induced transparency (EIT)-like transmission from Bull's-eye-shaped metamaterial [J]. Optics Express, 2010, 18(17): 17997-18002.
- [18] Ding J, Arigong B, Ren H, et al. Tuneable complementary metamaterial structures based on graphene for single and multiple transparency windows[J]. Scientific Reports, 2014, 4: 6128.
- [19] Hu S, Yang H L, Han S, et al. Tailoring dual-band electromagnetically induced transparency in planar metamaterials[J]. Journal of Applied Physics, 2015, 117(4): 043107.

- [20] Ning R X, Jiao Z, Bao J. Multi-band and wide-band electromagnetically induced transparency in graphene metasurface of composite structure [J]. IET Microwaves, Antennas & Propagation, 2018, 12 (3): 380-384.
- [21] Wang J Q, Fan C Z, He J N, et al. Double Fano resonances due to interplay of electric and magnetic plasmon modes in planar plasmonic structure with high sensing sensitivity [J]. Optics Express, 2013, 21(2): 2236-2244.
- [22] Zhang Y J, Wang S F, Zhong G C, et al. Metamaterial-based terahertz multi-band sensors integrated with microfluidic channels [J]. Chinese Journal of Lasers, 2019, 46(6): 0614038.  
张贇佳, 王少飞, 钟高超, 等. 微流控-超材料集成多带太赫兹传感器 [J]. 中国激光, 2019, 46(6): 0614038.
- [23] Li H Y, Liu J J, Han Z H, et al. Terahertz metamaterial analog of electromagnetically induced transparency for a refractive-index-based sensor [J]. Acta Optica Sinica, 2014, 34(2): 0223003.  
李化月, 刘建军, 韩张华, 等. 基于类电磁诱导透明效应的太赫兹折射率传感器 [J]. 光学学报, 2014, 34(2): 0223003.
- [24] Panahpour A, Silani Y, Farrokhan M, et al. Coupled plasmon-exciton induced transparency and slow light in plexcitonic metamaterials [J]. Journal of the Optical Society of America B, 2012, 29(9): 2297-2308.
- [25] Chen X D, Grzegorzczak T M, Wu B I, et al. Robust method to retrieve the constitutive effective parameters of metamaterials [J]. Physical Review E, 2004, 70(1 Pt 2): 016608.
- [26] Szabó Z, Park G H, Hedge R, et al. A unique extraction of metamaterial parameters based on Kramers-Kronig relationship [J]. IEEE Transactions on Microwave Theory and Techniques, 2010, 58 (10): 2646-2653.
- [27] Zhou J, Economou E N, Koschny T, et al. Unifying approach to left-handed material design [J]. Optics Letters, 2006, 31(24): 3620-3622.
- [28] Smith D R. Analytic expressions for the constitutive parameters of magnetoelectric metamaterials [J]. Physical Review E, 2010, 81(2): 036605.
- [29] Zhao R K, Koschny T, Soukoulis C M. Chiral metamaterials retrieval of the effective parameters with without substrate [J]. Optics Express, 2010, 18 (14): 14553-14567.
- [30] Li G S, Yan F P, Wang W, et al. Analysis of multiband and broadband electromagnetically induced transparency based on three-dimensional coupling [J]. Laser & Optoelectronics Progress, 2018, 55(12): 121601.  
李广森, 延凤平, 王伟, 等. 基于三维耦合的多波段宽带电磁诱导透明分析 [J]. 激光与光电子学进展, 2018, 55(12): 121601.
- [31] Ma C W, Ma W Y, Tan Y, et al. High Q-factor terahertz metamaterial based on analog of electromagnetically induced transparency and its sensing characteristics [J]. Opto-Electronic Engineering, 2018, 45(11): 180298.  
马长伟, 马文英, 谭毅, 等. 高 Q 值 THz 类 EIT 超材料及传感特性研究 [J]. 光电工程, 2018, 45(11): 180298.

## Design and Analysis of Electromagnetically Induced Transparency in THz Multiband

Zhang Min, Yan Fengping\*, Du Xuemei, Zhang Xiaoqi

Key Laboratory of All-Optical Network and Modern Communication Network of Ministry of Education, Institute of Lightwave Technology, Beijing Jiaotong University, Beijing, 100044, China

### Abstract

**Objective** Metamaterials have several advantages compared to natural materials. As they are produced by the artificial synthesis of periodic unit structures, metamaterials can achieve special electromagnetic phenomena, including electromagnetically induced transparency (EIT), near-zero refractive index, and photonic band gap. Therefore, improving the performance of metamaterials has become a hot topic in the industry. If metamaterial devices offer a rational selection of materials and structural parameter adjustment, their wide application in the field of terahertz technology would be possible. EIT is an optical quantum interference cancellation effect that makes opaque media transparent to light detection. It has substantial application value for the realization of slow light. In the atomic field, the conventional EIT effect requires strict experimental conditions, such as ultra-low temperature

and strong light pumping. However, when using metamaterials to achieve the EIT effect, only light and dark mode structures are needed. Their resonant absorption frequencies are quite similar. After an electromagnetic wave incident, light and dark mode structures are coupled with each other, and their transmission peak appears. Many researchers have studied and designed two-dimensional metamaterials, with a variety of different media and structures, and they have achieved ground-breaking results. However, only few studies have focused on three-dimensional (3D) metamaterials with the multi-band slow-light effect. In order to solve this critical problem, a 3D metamaterial model comprising of a square closed loop and split ring resonators is designed based on relevant principles. Moreover, the proposed structure shows a multiband EIT effect in the terahertz range.

**Methods** To design metamaterials with optimum performance, we first designed the unit structure, in which four split ring resonators were vertically arranged on the quartz substrate. In addition, the square closed loop was placed horizontally on the quartz substrate. The parameters of these four split ring resonators were the same, and the opening positions were forward and reverse. Next, we used CST to simulate an EIT metamaterial structure and study its mechanism. For analyzing the mechanism of its electromagnetic response and EIT effect, we split the metamaterial structure into reverse and forward double-split ring resonator unit structures that were then simulated and compared. In addition, to further explore the mechanism of resonance peaks, the electric and magnetic field distributions (at each resonance peak) were analyzed. The structural parameters, including the width, opening size, and square closed loop size, were analyzed and studied. Finally, the optical buffer was studied, and the proposed structure was applied to the refractive index sensor.

**Results and Discussions** The designed metamaterial structure has four transmission peaks at 1.21 THz, 1.46 THz, 1.61 THz, and 1.98 THz. The coupling bodies of the bright mode and dark mode in the structure are forward and reverse double split ring resonators, respectively with a square closed loop, respectively, and the resonance intensity is about 0.90 (Fig. 2). Compared with the customary structure, the proposed structure achieves a four-band, high-intensity EIT effect. The first resonance transmission peak appears at 1.21 THz, which infers that the forward and reverse double split ring resonators and the square closed loop are light and dark modes of one another. It can also be inferred that they are coupled after the magnetic wave incident (Fig. 3). The second transmission peak appears at 1.46 THz, which is obtained by the coupling of the forward double split ring resonators and the square closed loop as light and dark modes of each other (Fig. 3). The third transmission peak is pinpointed at 1.61 THz, which is obtained by the coupling of four split ring resonators and the square closed loop, also as bright and dark modes of each other (Fig. 3). The last transmission peak appears at 1.98 THz, which indicates that it is obtained by the coupling of the reverse, double split ring resonators, and the square closed loop. In the discussion of broadband EIT characteristics, by differentiating the absorption peaks, the split ring resonators are sharper than the square closed loop, so the electromagnetic resonance is more intense and the value is also elevated. The forward double split ring resonators and the square closed loop are of mutual light and dark modes, and they are coupled to form two transmission peaks with a bandwidth of 0.25 THz. In the same way, the reverse double split ring resonators and the square closed loop are also coupled, forming two transmission peaks with a bandwidth of 0.52 THz and 0.41 THz. The simulation results show that the broadband characteristics have clear advantages over the 0.1 THz bandwidth of the traditional narrow-band structure (Fig. 4). For the opening size of the split ring resonators, the resonance intensity of the EIT transmission peak decreases simultaneously with the increase of parameters, and the bandwidth also decreases (Fig. 5). For the size of the square closed loop, the resonance intensity of the transmission peak gradually increases along with the successive increase of the transmission peak. This reveals a small blue shift of the transmission peak, and the bandwidth also increases (Fig. 6). For research in the field of optical buffering, with the rapid increase of refractive index and dispersion, the group refractive index also increases in the EIT effect. The values are 67.6, 37.5176.4, and 57.8289.4 (Fig. 7). Finally, when the proposed structure is applied to the refractive index sensor, the refractive index sensitivities of four bands are 235.2, 39.2, 65.8, and 29.4 GHz/RIU, respectively. In contrast with the conventional EIT structure, the designed metamaterial structure not only presents multiband refractive index sensing performance but also presents its own high sensitivity (Fig. 8).

**Conclusions** The results show that the EIT effects of 1.21 THz, 1.46 THz, 1.61 THz, and 1.98 THz can be achieved in the three-dimensional structure model of metamaterials in terahertz band; the resonance intensity can reach 0.90, 0.89, 0.90, and 0.87, respectively. The mechanism of the multiband EIT resonance was studied by differentiating the coupling response of forward and reverse double split ring resonators, and a square closed loop.



By adjusting the structural parameters, the influence of the size of the opening of the split ring resonators and the size of the square closed loop on the strength and bandwidth of the EIT (in the metamaterial) is discussed. Compared with the traditional design, the metamaterial 3D structure indicates a multiband EIT effect, and it shows an escalating refractive index sensitivity in multiple bands. This can produce a strong slow-light effect at multiple frequency points. Therefore, it is satisfactory for the application and promotion in the field of refractive index sensing and optical buffer.

**Key words** material; metamaterials; electromagnetically induced transparency; multi-band; terahertz; slow light effect

**OCIS codes** 160.3918;300.6495;230.5750; 280.4788